

## Anomalous fluorescence line intensity in megavoltage bremsstrahlung

M. S. Litz,<sup>1</sup> G. Merkel,<sup>1</sup> N. R. Pereira,<sup>2,a)</sup> C. N. Boyer,<sup>3</sup> G. E. Holland,<sup>4</sup> J. W. Schumer,<sup>5</sup> J. F. Seely,<sup>5</sup> L. T. Hudson,<sup>4</sup> and J. J. Carroll<sup>6</sup>

<sup>1</sup>Army Research Laboratory, 2800 Powder Mill Rd., Adelphi, Maryland 20873, USA

<sup>2</sup>Ecopulse, Inc., P.O. Box 528, Springfield, Virginia 22150, USA

<sup>3</sup>L3-Communications, Washington, DC 20375, USA

<sup>4</sup>National Institute of Standards and Technology, Gaithersburg, Maryland 20899, USA

<sup>5</sup>Naval Research Laboratory, Washington, DC 20375, USA

<sup>6</sup>Physics and Astronomy, Youngstown State University, Youngstown, Ohio 44555, USA

(Received 11 January 2010; accepted 22 March 2010; published online 28 April 2010)

An anomalous ratio between  $K\alpha$  and  $K\beta$  fluorescence interpreted with plasma radiation modeling can be a useful diagnostic in laser-produced plasmas. In cold tungsten there exists a similar but as yet undocumented anomaly: for 2 MeV end point bremsstrahlung in the forward direction  $K\beta/K\alpha_1 \approx 1$ , while this ratio is closer to 0.5 for bremsstrahlung in reflection and for an isolated atom. As in the laser-produced plasma, the anomalous ratio reflects a localized source of fluorescence inside the material combined with differential attenuation of the fluorescence photons on their way out. To measure the  $\approx 60$  keV fluorescence lines, a Cauchois transmission crystal spectrograph that works well for laser-produced plasmas must suppress the intense bremsstrahlung that accompanies the fluorescence, by beefing up marginal shielding and avoiding extraneous scatter sources. © 2010 American Institute of Physics. [doi:10.1063/1.3389226]

### I. INTRODUCTION

Plasma spectroscopy<sup>1</sup> is a basic diagnostic for hot plasmas. The x-ray spectrum is determined by the plasma's density, temperature, and size, and numbers can be assigned to these quantities by matching the spectra calculated by plasma radiation models with measured x-ray spectra. Heliumlike lines from the K-shell are especially helpful because it is well understood how the plasma affects their detailed energies, strengths, and shapes. Fluorescence radiation, the  $K\alpha$  and  $K\beta$  photons emitted from the K-shell, can be equally useful. In one recent example, implicit-hybrid particle-in-cell simulations coupled to a collisional-radiative code could determine a laser-produced plasma's bulk temperature.<sup>2</sup> In another example, an anomalous ratio between fluorescence lines suggested<sup>3</sup> that the laser deposited its energy deep inside the plasma.

A much simpler situation than a laser-produced plasma is cold-target bremsstrahlung, but here the fluorescence line ratio can also be anomalous and indicate where the fluorescence comes from. Neutral atoms emit  $K\alpha$  and  $K\beta$  photons in the ratio  $K\beta/K\alpha_1 \approx 0.41$ .<sup>4</sup> However, the ratio  $K\beta/K\alpha_1$  in 2 MeV end point forward bremsstrahlung turns out to be  $\approx 1$ , a fact that has not yet been documented earlier.

The instrument that makes this observation possible is a Cauchois transmission crystal spectrometer modified for the purpose. Originally designed for a medical application,<sup>5</sup> the instrument works very well with laser-produced plasmas<sup>6</sup> and continues to be improved for this and other high-fluence applications. For the same purpose the recent literature contains simpler<sup>7</sup> transmission spectrometers and more elaborate instruments for use with low-flux sources<sup>8</sup> with a similar design.

Exercising the Cauchois transmission x-ray spectrograph with 2 MeV bremsstrahlung is to prepare for measurements of plasmas at the Naval Research Laboratory on a 6 MeV pulsed power generator, Mercury.<sup>9</sup> Its other parameters include a 400 kA peak current with 25 ns width that contains about 10 mC. A complementary but less demanding test source is the plasma-filled rod pinch:<sup>10</sup> an upgraded spectrometer tested on this source gives good results that will be published elsewhere.<sup>11</sup>

The test bed is a Varian L200A linear accelerator that produces 2 MV end point<sup>12</sup> bremsstrahlung in 5  $\mu$ s bursts at about 200 Hz. The average current is around 0.15 mA, accumulating 10 mC in about a minute. In radiation from a fully stripped plasma the K-shell photons often dominate the radiation, but in megavoltage bremsstrahlung the K-lines are a minor component, especially in the forward direction. The spectrum's hard photons tend to scatter many times in the shielding before they disappear, so that background suppression must be done carefully for the K-lines to become visible. Intense bremsstrahlung should be expected also from plasmas made on the National Ignition Facility (NIF), so that the results in this paper add confidence to the feasibility of diagnosing high-energy K-shell radiation on NIF with this type of Cauchois transmission spectrograph.

Figure 1 shows two spectra computed for 2 MeV end point bremsstrahlung, in the geometry of Fig. 2. Monoenergetic 2 MeV electrons from the left enter a 0.8 mm tungsten converter along the axis. The black line is the number spectrum in a silicon absorber on the axis 100 mm in front of the converter. The red line is the backward spectrum, again computed in silicon 100 mm back from the converter. The bremsstrahlung continuum dominates both number spectra. In the backward direction the continuum is relatively soft, but the spectrum in the forward direction is dominated by harder x

<sup>a)</sup>Electronic mail: pereira@speakeasy.net, URL: <http://www.ecopulse.com>.

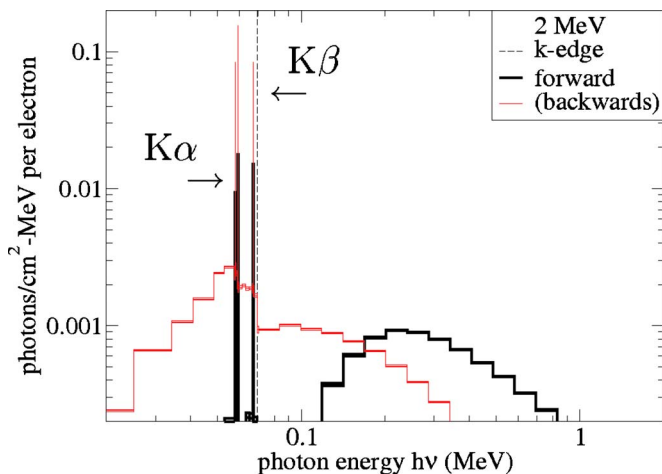


FIG. 1. (Color online) The photon number spectrum computed with ITS for normally incident 2 MeV electrons on a CSDA-range thick bremsstrahlung target, in the geometry of Fig. 2. The pair of thick black lines indicated by  $K\alpha$  are the  $K\alpha_2$  fluorescence line (to the left), and the  $K\alpha_1$  line (to the right) in the forward direction: the thin, long single line indicated by  $K\beta$  is the single fluorescence line that ITS uses to represent the three  $K\beta$  lines, in the backward direction.

rays, in this figure from 0.8 MeV down to 120 keV where the influence from tungsten's K-edge becomes visible.

This paper deals with K-shell fluorescence, represented by vertical lines in the spectrum's histogram. All computations use the ACCEPT member of ITS' standard version.<sup>13</sup> This simplifies tungsten's K-shell fluorescence to two L-shell lines,  $K\alpha_1$  at 59.320 keV and  $K\alpha_2$  at 57.983 keV, and a single  $K\beta$  line at 67.246 keV that represents all other K-shell transitions. The K-edge is at 69.5250 keV. The energy bins for the fluorescence are chosen to be 0.2 keV wide, which allows fluorescence and bremsstrahlung, in logarithmically increasing bins, to have the same vertical scale. Occasionally the top line in the histogram is double, suggesting the computation's statistical accuracy. This is always better than a few percent.

High atomic number atoms whose K-shell is ionized relax over 95% of the time by emitting a K-shell fluorescence photon.<sup>4</sup> For every 100 $K\alpha_1$  photons there are 58 $K\alpha_2$  and 41 $K\beta$  photons, hence it is no surprise to find the ratio  $K\alpha_2/K\alpha_1 \approx 0.5$ , both in the backward and forward number spectra. The same is true for  $K\beta/K\alpha_1$  in the backward direction, the thin red line in Fig. 1. The ratio  $K\beta/K\alpha_1 \approx 0.5$  also, and the combined  $K\beta$  line is just as intense as the  $K\alpha_2$  line. In contrast this with the forward direction, where the  $K\beta$  radiation is almost as strong as the  $K\alpha_1$  line and substantially stronger than  $K\alpha_2$ .

Quite apart from the line ratios, fluorescence is most intense in the backward direction. X-ray crystallography

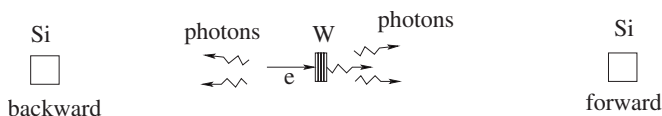


FIG. 2. Computational geometry for the spectra in Fig. 1, backward with respect to the electrons, reflection, and forward, transmission.

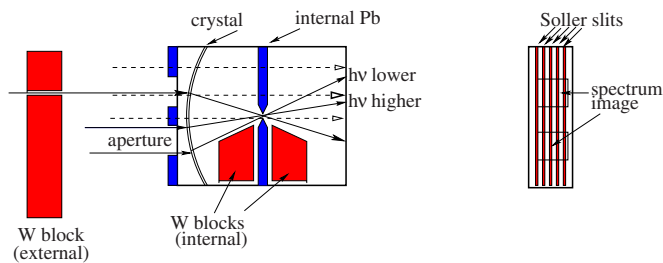


FIG. 3. (Color online) Sketch of the relevant spectrometer components.

with line radiation is therefore always done in a reflection geometry. A comprehensive review<sup>14</sup> discusses this topic for low-energy electrons in the context of electron probe microanalysis. Relatively low-intensity bremsstrahlung spectra and the embedded fluorescence can be measured quite well by counting the photons.<sup>15</sup>

Photon counting cannot be done when the radiation is too intense. It is then much more difficult to measure the spectrum of hard bremsstrahlung or bremsstrahlunglike radiation:<sup>16</sup> usually, calculations must suffice. To date the fluorescence lines in intense, megavolt bremsstrahlung do not seem to have been observed, and computations that mention the relatively high intensity of the more energetic  $K\beta$  photons compared to the dominant  $K\alpha_1$  radiation in forward bremsstrahlung do not seem to exist either.

Bremsstrahlung computations confirm that the anomalous  $K\beta/K\alpha_1$  ratio comes in part from differential absorption, the cold-material analog of opacity in a hot plasma. However, differential absorption becomes noticeable only when the fluorescence is generated far enough away from where the radiation emerges. This happens for megavolt electrons in high atomic number materials, in which electron scattering off nuclei is more effective in impeding electrons from penetrating into the material than the slow, continuous energy loss due to electron-electron collisions. As mentioned, anomalous fluorescence line ratios observed recently in spectra from layered targets irradiated by an intense femtosecond laser<sup>3</sup> were tentatively attributed to a similar cause, a fluorescence source deep inside the plasma.

## II. EXPERIMENTAL RESULTS

The center part of Fig. 3 is a top view of the spectrometer.<sup>6</sup> The crystal for the present measurement is Ge 220, cylindrically bent to a 254 mm radius on a substrate that is not shown. It focuses the x rays on the Rowland circle where an image plate registers the spectrum. The solid lines suggest the x-ray paths in normal operation. They pass through two apertures to two nominally identical parts of the crystal, which diffracts the radiation to give two nominally identical spectra. The lower-energy x rays diffract over a larger angle and end up toward the spectrometer's outside; the harder x rays remain closer to the center line. The distance between the lines directly translates into photon energy.

The dashed lines shown only in the figure's upper part indicate leakage x rays that pass through the spectrometer's standard 19 mm lead aperture, the crystal, and the 19 mm

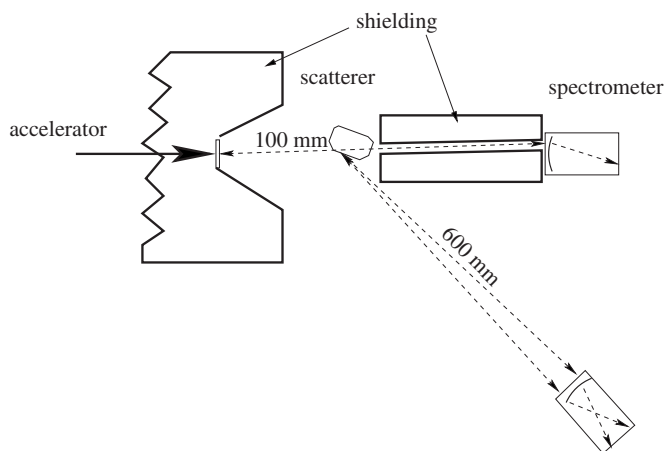


FIG. 4. The spectrometer's location in the direct radiation from the L200A linac (top) and in the reflection geometry (bottom). Shielding is schematically indicated by the thick lines. The scatterer is on-axis, about 100 mm from the converter.

lead internal shielding around the x rays' crossover point inside the spectrometer itself. X rays leaking through and around the upper aperture overlap with the x-ray spectrum made by x rays that came through the lower aperture, and vice versa. In this particular spectrometer geometry it proved essential to suppress leakage x rays with an additional shield, the tungsten block shown on the left side in Fig. 3.

The entrance aperture determines the spectrometer's photon energy range. The range is from 27 to 165 keV with the standard aperture fully open and the x-ray source 600 mm from the crystal on the instrument's center line. Otherwise, when the alignment is off, the hardest and/or softest x rays that graze the internal shielding around the crossover region can be cut off. The spectrometer's energy range also becomes smaller if the aperture is made narrower.

In hard bremsstrahlung the continuum is much stronger than the fluorescence lines, and a small fraction of hard photons scattering or otherwise penetrating into the spectrometer can cause major problems. To minimize scattering any structure illuminated by direct bremsstrahlung should be avoided, except of course the crystal whose full illumination is essential to have the maximum energy range. Some background radiation can be useful: K-edge filters across the crossover region give a convenient energy calibration when the background is soft enough and low enough, as it is for many laser-produced plasmas. A hard bremsstrahlung background is useless even when it is low enough.

The shielding added to make the present measurement possible is represented by the red tungsten blocks in Fig. 3. Two 50 mm thick trapezoidal blocks (shown only on the lower side) beef up the original 19 mm lead shield, but these two shields are insufficient: they must be supplemented by external shielding in front of the aperture. The tungsten block to the left in the figure is most effective as shown, when it defines a second, smaller aperture that illuminates the bent crystal only where it diffracts the desired x rays. Figures 3 and 4 omit the 100 mm thick lead shield that surrounds the spectrometer, from crystal to image plate, and also protects the x-ray path from source to the spectrometer entrance.

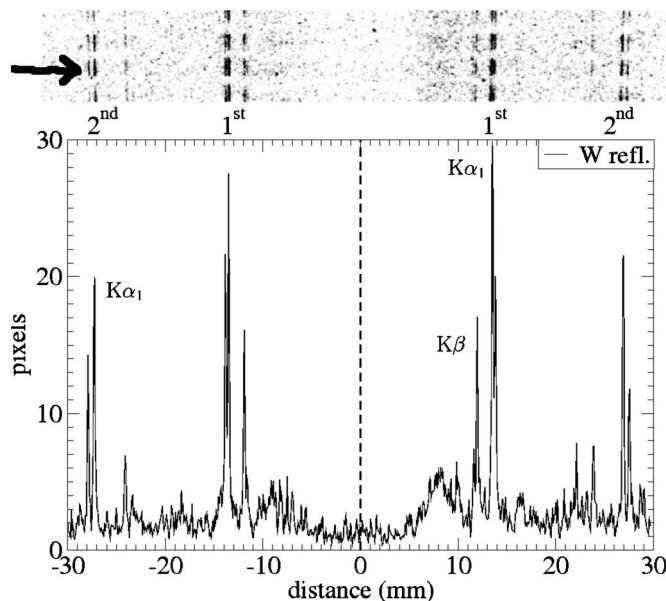


FIG. 5. The x-ray spectrum from tungsten excited by 2 MeV bremsstrahlung as seen on the image plate (top) and the average intensity over the spectrum indicated by the arrow.

Shielding inside the spectrometer attenuates the hard x rays in part by scattering, hence internal shielding directly illuminated could add a background of scattered x rays. In an attempt to suppress such scatter, the spectrometer complements the standard internal shielding with Soller slits. The right side of Fig. 3 looks at the spectrometer's back. It shows the Soller slits, and where the images of the spectrum register on the image plate.

Soller slits are thin sheets of an x-ray absorbing material, here tungsten, placed parallel to the paths of the desired x rays. The tungsten sheets are held in place with tungsten wedges, in the same position as the trapezoidal tungsten blocks in Fig. 3. The diffracted x-ray path is then restricted to a narrow tungsten cone, and x rays that hit the cones' sides suffer multiple scatterings and are eventually lost. The Soller slits turn out to be less functional than originally expected.

Figure 4 sketches two measurement geometries. In both geometries the electrons from the Varian L200A accelerator, to the left, hit a tungsten converter at the apex of an open-cone shield made from depleted uranium. In direct bremsstrahlung the spectrometer sits 600 mm in front of the converter on the axis, but without the scatterer: however, one aperture is blocked by a long tungsten shield (shown as a block in Fig. 3).

In the photofluorescence setup the accelerator's bremsstrahlung illuminates a scatterer  $\approx 100$  mm behind the converter: the radiation-excited fluorescence and any scattered radiation enter the spectrometer shown at the figure's bottom, now 600 mm away from the scatterer. In this setup both apertures in the spectrometer can be open because the continuum radiation is benign.

Figure 5 gives a spectrum from a tungsten scatterer, illuminated for  $\approx 10$  min by 2 MeV end point bremsstrahlung. The four sample spectra seen on top of the figure are spectral lines cut by the Soller slits. The lines are approximately

TABLE I. Some data for tungsten's k-shell (Ref. 4).

Line	ITS	Energy (keV)	$P_n$	$\mu/\rho$ (cm <sup>2</sup> /g)	$\phi_n$	W	W-Cu
$K\alpha_2$	L3-K	57.983	0.58	4.06	0.54	0.52	0.46
$K\alpha_1$	L2-K	59.320	1.00	3.82	1.00	1.00	1.00
$K\beta_3$		66.951	0.11	2.81			
$K\beta_1$	Valence-K	67.244	0.22	2.78	0.41	0.85	1.14
$K\beta_2$		69.067	0.08	2.60			
K-edge		69.525					

symmetric left to right, with small differences that could come from a minor misalignment, unintended asymmetries between the two sides of the crystal, or differences in the image plate's response on the two sides. The four inter-Soller spectra are approximately the same within the image's noise level, but the spectral lines are not perfectly parallel to each other: apparently, the image plate was not exactly perpendicular to the x rays.

Although some pixels away from the spectral lines are just as dark as those inside the lines, the overall noise level is acceptable: the spectrometer's internal shielding is adequate for scattered bremsstrahlung and the photo-fluorescence it excites. The image on top of Fig. 5 covers an area of  $70 \times 14$  mm<sup>2</sup>, a small part of a much larger ( $422 \times 200$  mm<sup>2</sup>) image plate. The short lines in each of the four spectra are 1.8 mm high.

Each side has lines in two diffraction orders. In the first order of diffraction, the two spectra closest to the center, the intensity is higher and the dispersion half that of the spectra in second order, toward the outside. In first order the  $K\beta$  line at 66.95 keV is 2 mm to the right of the  $K\alpha_2$  line at 57.98 keV (on the left-hand spectrum): the dispersion is  $\approx 4.5$  keV/mm, and two  $\approx 0.1$  mm pixels (300 pixels/in.) are 450 eV apart. In second order the dispersion doubles, to  $\approx 2.4$  keV/mm.

The lower part of Fig. 5 is the average pixel value of the spectral slice indicated by the arrow. In first order the 66.95 keV  $K\beta$  line is at 12.1 mm, while the  $K\alpha_1$  line is at 13.6 mm and  $K\alpha_2$  at 13.8 mm: their energies are 59.32 and 57.98 keV (see Table I). The length scale has been symmetrized for the  $K\alpha_1$  lines, so that the  $K\alpha_1$  line on the left side is exactly at  $-13.6$  mm. The  $K\beta$  line at  $-11.7$  mm is not quite symmetric, and the  $K\beta$  spectrum has one line on the left and two on the right although they are all barely above background. The various asymmetries do not affect the overall results, but they could become problematic in attempts at a detailed comparison with computations.

For this photoexcited spectrum the  $K\beta$  line in first order is about half as intense as the  $K\alpha_1$  line and slightly larger on the right side than on the left. How the  $K\alpha_2$  relates to the  $K\alpha_1$  line is not clear from the first order spectrum since the first order dispersion is insufficient to separate the lines.<sup>17</sup> However, on the right the second order spectrum suggests  $K\alpha_2/K\alpha_1 \approx 0.5$ , while the ratio is closer to 0.7 on the left. Given the statistical variation, in data and background, these line ratios are close enough to the standard value of 0.5.

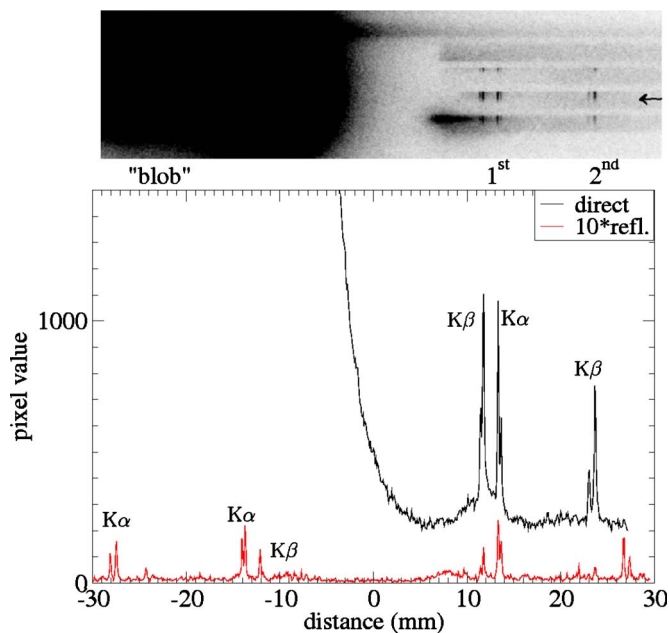


FIG. 6. (Color online) A forward-directed bremsstrahlung spectrum from the 2 MeV end point linac. The bottom part is average pixel value of the spectrum slice indicated by the arrow.

The top section of Fig. 6 is an image produced by forward-directed bremsstrahlung made by  $\approx 27$  mC in 2 MeV electrons. At the spectrometer's entrance aperture the dose is about 27 Gy.

In the reflection geometry the spectrometer gives two symmetric spectra, but with direct bremsstrahlung only a single spectrum can be obtained. One spectrometer aperture must be blocked with an external shield, so that the spectrum from the open aperture is not swamped by the x rays that pass through the other aperture, the crystal, and the internal shielding as illustrated by the dashed lines in Fig. 3. Undiffracted x rays that pass through the unshielded aperture create the blob on the left side in Fig. 6.

In the image on top of Fig. 5, for reflected radiation, the four separate Soller slit spectra seem substantially similar, but in the image on top of Fig. 6, for direct radiation, the four spectra are quite different. The top Soller slit spectrum is absent, and all spectra are most intense on the upper side. The vertical asymmetry comes from imperfect alignment of the Soller slits with the nominally 2 mm high radiation source, whose position on the 9 mm diameter converter is not known *ab initio*. Hardware and time did not allow subsequent adjustment. The feature in the lower spectrum on the high-energy side of the fluorescence is a radiation leak: high-energy bremsstrahlung there would exist in the second order spectrum too.

The black line in the bottom part of Fig. 6 is the average pixel value for the spectrum at the arrow in the image at the top. With its maximum around 30 000 the blob on the left is 20 times off scale: the spectrum on the right, with a pixel value around 1000, would have been obliterated if radiation could have come in unimpeded through the blocked-off aperture. With about 25% of the exposure time, the forward fluorescence lines in Fig. 6 are two orders of magnitude

larger than those from the radiation-excited spectrum in Fig. 5. The red line at the bottom is the latter spectrum, multiplied tenfold and aligned with the first order  $K\alpha_1$  line in forward fluorescence.

In first order the dispersion is too small to separate the  $K\beta$  line's three components, while in second order the  $K\beta_2$  line is separated by  $\approx 0.7$  mm from the  $K\beta_1$  line that still contains the  $K\beta_3$ . In second order the direct fluorescence spectrum has the  $K\beta$  line but lacks the  $K\alpha$  lines, indicating a misalignment in the horizontal direction that restricts the aperture on the outside where the bent crystal diffracts the lower-energy photons.

In the fluorescence spectrum from irradiated tungsten, in Fig. 5 and in the red line at the bottom of Fig. 6, the  $K\alpha_1$  line is twice as strong as the  $K\beta$  line as expected for an individual tungsten atom. However, in the forward spectrum of Fig. 6 the  $K\beta$  line is slightly larger than the  $K\alpha_1$ . The background is about 20% and gives some minor differences in the ratio between the two  $K\alpha$  lines: without subtracting the background  $K\alpha_2/K\alpha_1 \approx 0.59$ , with background subtraction it is  $\approx 0.47$ . Both are close to the standard  $K\alpha_2/K\alpha_1 \approx 0.5$ .

In the upper part of Fig. 6 the background behind the Soller slits is visibly lower than in between the Soller slits, under the spectra, but the difference is only about 30%. Along the spectral lines the background behind the Soller slits is about the same as just outside the spectral lines. Therefore, the background must be from hard radiation, for which the Soller slits are ineffective. The Soller slits do, however, cut off the lower-energy fluorescence.

The hard bremsstrahlung background becomes smaller when fewer hard photons get into the spectrometer. One way to do this is to make the aperture smaller, more like a vertical slit. For a survey spectrometer a narrow slit is counterproductive because it limits spectral coverage, but for the intended application (and for a bremsstrahlung monochromator<sup>18</sup>) the x rays of interest are known in advance. A narrower slit demands better alignment, otherwise the radiation of interest may be cut off. Imperfect alignment can already be an issue when the aperture is open, viz., the lack of  $K\alpha$  lines in second order in Fig. 6.

The blue line in Fig. 7 is the forward spectrum when the entrance slit is narrowed to 3 mm, added to the same data as the bottom panel in Fig. 6, where the aperture is  $\approx 14$  mm wide. For the 3 mm thin slit the crystal diffracts tungsten's K-shell fluorescence in first order only. The blue spectrum in Fig. 7 is stronger than the spectrum in Fig. 6 in proportion to a slightly longer exposure time, but the blob on the left and the background under the spectral lines are both substantially smaller than before, consistent with the fourfold smaller aperture. The ratio  $K\beta/K\alpha_1 \approx 1.05$  is unchanged. Improving the alignment together with further tightening of the aperture could not be explored because the experiment had to stop for reasons beyond our control.

To our knowledge, the fluorescence in forward-directed radiation has not yet been observed in the megavoltage regime, and the anomaly in the intensity ratio  $K\beta/K\alpha_1 \approx 1.05$  rather than the usual  $\approx 0.5$  has therefore escaped detection. One obvious reason is differential attenuation: photoelectric absorption is roughly proportional to  $1/(h\nu)^3$  and

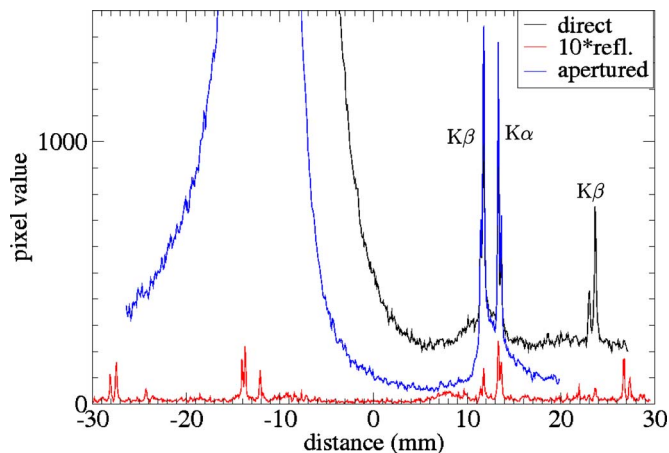


FIG. 7. (Color online) The x-ray spectrum at the arrow in Fig. 6 added to the data in the bottom part of Fig. 6.

the  $K\beta$  photons have higher energy  $h\nu$  than the  $K\alpha$  photons. However, differential attenuation comes into play only when the principal source of K-shell photons is localized on the converter's inside, away from where the radiation comes out, and when the continuum radiation does not produce too much fluorescence beyond the primary source. Section III corroborates this description with computations of the radiation production.

### III. FLUORESCENCE LINE RATIO COMPUTATIONS

Table I summarizes some data<sup>4</sup> for tungsten's K-shell. The strongest line is the  $K\alpha_1$  line, in ITS designated as L2-K, followed by the  $K\alpha_2$  line, or L3-K: ITS' names explicitly connect the fluorescence x ray to the shell transition. The  $K\beta$  lines correspond to transitions from higher-lying shells ( $K\beta_1$  and  $K\beta_3$  from the M-shell and  $K\beta_2$  from the N-shell). ITS' standard version limits itself to the two  $K\alpha$  lines and merges all the  $K\beta$  lines into a single line with energy 67.246 keV, valence-K.

The fluorescence photons are emitted with the relative probabilities  $P_n$  or branching ratios given in column 4, with the index  $n$  distinguishing the different lines. In ITS the single  $K\beta$  line has a probability  $P_{123}=0.42$ , consistent with the individual probabilities in Table I.

X-ray attenuation can be ignored for a thin foil, in which case the fluorescence line intensities are proportional to the probabilities  $P_n$ . For a thick foil the intensities change due to attenuation, with well-known self-attenuation factors that depend on geometry and further on the mass attenuation coefficient. The fifth column gives tungsten's mass attenuation coefficient  $\mu/\rho$  for the various fluorescence x rays. Tungsten's high density,  $\rho=19.3$  g/cm<sup>3</sup>, makes the attenuation length,  $\ell=(\mu/\rho)^{-1}/\rho=1/\mu$ , short, about 0.12 mm for the  $K\alpha$  x rays and 35% longer for  $K\beta$  x rays.

Electrons penetrate into a material at most up to the continuous slowing down approximation (CSDA) range, and the computations below are done for range-thick bremsstrahlung converters. For a 2 MeV electron in tungsten the CSDA

range is 1.6 g/cm<sup>2</sup>, a mass per unit area that transmits only about 1% of the K $\beta$  fluorescence and 0.2% of the K $\alpha_1$  radiation.

Self-absorption of fluorescence x rays in a range-thick bremsstrahlung converter must be small when the inverse CSDA range is smaller than the fluorescence's mass attenuation coefficient ( $\mu/\rho$ ). For tungsten K $\alpha_2$  with ( $\mu/\rho$ )  $\approx$  4 cm<sup>2</sup>/g the inverse CSDA range corresponds to a 0.4 MeV electron. Below a 0.4 MeV end point energy the ratio K $\beta$ /K $\alpha_1$  in bremsstrahlung from tungsten should then be K $\beta$ /K $\alpha_1$   $\approx$  0.5, in both the forward and backward directions. Most dc x-ray sources have end point voltages below 0.5 MV, and anomalies in the ratio K $\beta$ /K $\alpha_1$  have not been reported.

In a one-dimensional approximation, a K-shell ionization profile  $K(x)$  at a distance  $x$  from the surface at  $x=0$  in a thin slab  $dx$  produces fluorescence photons of type  $n$  proportional to  $P_n K(x) dx$ . For a slab with thickness  $d$  the fluence coming out of the material is then

$$\phi_n = P_n \int_0^d dx \exp(-x/\ell_n) K(x). \quad (1)$$

When the material is much thicker than the attenuation length, and the K-shell ionization is constant,  $K(x)=K_0$ , the fluence is simply

$$\phi_n = K_0 P_n \int_0^\infty dx \exp(-x/\ell_n) = K_0 P_n \ell_n = \frac{K_0 P_n}{\rho} \frac{1}{(\mu/\rho)_n}. \quad (2)$$

Here the index  $n$  stands for  $\alpha_2$ ,  $\alpha_1$ , or  $\beta$ . The attenuation factor is more complicated but still analytically tractable when the material has a finite thickness, when the ionization profile is an exponential, and when the photons enter and exit under an angle. Factors of the form  $1 - \exp[-x_b/(\ell_n \cos \theta)]$  then account for the missing fluorescence beyond  $x_b$  and for photon propagation under an angle  $\theta$  with the normal. When off-normal propagation is ignored, an exponential ionization profile  $\exp(-x/\ell)$  in a thick slab gives for the relative intensity  $\phi_\beta$  of the K $\beta$  line with respect to  $\phi_\alpha$  of K $\alpha_1$ ,

$$\frac{\phi_\beta}{\phi_\alpha} = \frac{P_\beta}{P_\alpha} \left[ \frac{(\mu/\rho)_{\alpha_1} - (\mu/\rho)_i}{(\mu/\rho)_\beta - (\mu/\rho)_i} \right], \quad (3)$$

where the scale length  $\ell$  defines an effective mass attenuation coefficient  $(\mu/\rho)_i = 1/(\ell\rho)$ .

An exponential profile applies when ionization is done by monoenergetic photons,<sup>19</sup> provided that Compton scatter is unimportant and no radiation buildup takes place (which is not always obvious). According to this formula K $\beta$ /K $\alpha_1$  can take on any value by selecting the ionization gradient  $(\mu/\rho)_i$  and the energy  $h\nu_i$  of the irradiating photons. In tungsten  $(\mu/\rho)_i = 2.4$  cm<sup>2</sup>/g for  $h\nu_i = 126$  keV and the fluorescence ratio K $\beta$ /K $\alpha_1$  would be close to unity. Irradiating a thick slab of tungsten with the K $\alpha_1$  line from gold, at  $h\nu_i = 68.8$  keV, should give a similar ratio of (very weak) fluorescence photons.

Figure 8 illustrates a few dependencies versus depth in a range-thick (0.8 mm) tungsten slab. Fluorescence generated

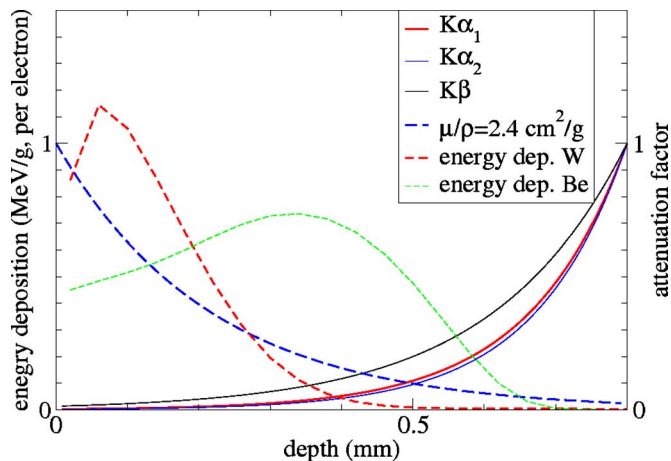


FIG. 8. (Color online) Attenuation of tungsten fluorescence lines in tungsten and some relevant excitation profiles.

at a particular depth comes out of the back of the material exponentially attenuated. The solid lines are the transmission factors for the K-lines, with the mass attenuation coefficients from Table I. The blue dashed line indicates exponential ionization with  $(\mu/\rho)_i = 2.4$  cm<sup>2</sup>/g, when K $\beta$ /K $\alpha_1$  should be about unity.

For electrons the ionization as function of penetration depth is best computed numerically, with Monte Carlo codes such as ITS: there is no convenient analytical form. While ITS keeps track of the K-shell fluorescence generation internally, in the standard output from ITS the quantity most closely related to the fluorescence source is energy deposition.

The dashed red line in Fig. 8 is the energy deposition for monoenergetic 2 MeV electrons in tungsten. Tungsten's nuclei scatter the electrons so strongly that very few reach the end of the CSDA range. In this computation the largest energy loss is at about 1/8 of the CSDA range and the electrons have lost the bulk of their energy in the converter's first half. Almost no hard bremsstrahlung is produced in the second half. For this reason bremsstrahlung converters often consist of a bremsstrahlung-generating high atomic number in front, and a low atomic number material in the back that attenuates the x rays less.

In low-atomic number materials the electrons are unhampered by scattering, and they penetrate deeper. The green dashed line is the energy deposition for a material with the same CSDA range as tungsten but with reduced nuclear charge, such as water or beryllium (as shown). Measuring the depth-dose profile in a water phantom is a standard way to determine electron energy in the megavolt range, where x-ray filtering does not work (but other methods do<sup>12</sup>).

Most of the K-shell fluorescence in tungsten comes from photoionization by bremsstrahlung photons with energies  $h\nu > h\nu_K$ , close to the K-edge  $h\nu_K$ . These photons are strongly absorbed, approximately as  $1/(h\nu)^3$ . They are also generated efficiently, since bremsstrahlung production varies more or less as  $1/h\nu$ . K-shell photoionization is then most important for photons between  $h\nu_K$  and some Compton scattering limit  $h\nu_C$ , where the photoelectric cross section becomes comparable to the cross section for Compton scatter:

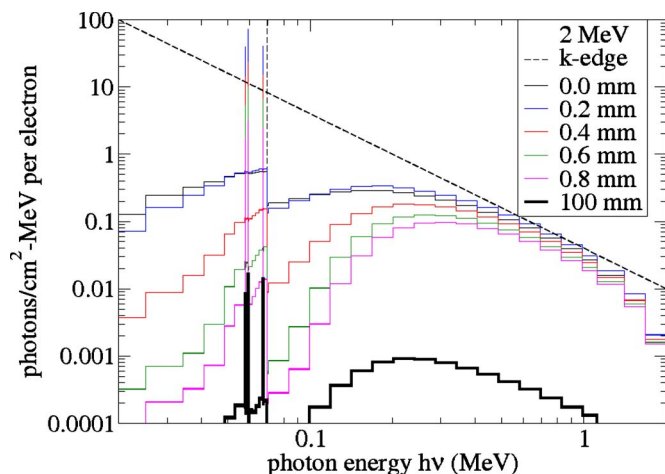


FIG. 9. (Color online) Local photon number spectrum in a range-thick tungsten converter (thin lines) and the spectrum emerging from the back side (thick black line).

scattering lowers the photon's energy so that it is absorbed more readily.

The column marked W in Table I gives the relative intensity  $I_n = \phi_n / \phi_{\alpha_1}$  from Fig. 1, forward bremsstrahlung from 2 MeV electrons normally incident on range-thick tungsten. The relative intensity computed for  $K\beta$  fluorescence is  $I_\beta \approx 0.85$ , lower than the measured value  $I_\beta \approx 1.05$  but already much larger than for thin tungsten,  $I_\beta \approx 0.41$ , or the value  $I_\beta \approx 0.55$  for a constant ionization profile corrected by the ratio of the mass attenuation coefficients.

The discrepancy between this computation and the measurement may come from converter composition. The design of the converter for the Varian L200A was not available, hence the computation in Fig. 1 assumed the simplest case, range-thick solid tungsten. The K-line energy confirms that tungsten is the converter's high atomic number component, but the spectrometer cannot see lower-energy lines from lower atomic number materials in the converter's back. It is likely, however, that the converter has the same design as in other Varian linacs, a thin tungsten layer in front backed up with copper to remove the heat. Likewise, converters optimized for dose deposition in silicon typically have 1/3 of their mass per unit area in some high atomic number material (often tantalum), while the remainder is some low atomic number material (usually carbon or plastic).

The largest fluorescence ratio in the computations results when the second half of the tungsten is replaced by the same mass per unit area copper,  $I_\beta \approx 1.14$  in the last column of Table I marked W-Cu. The experimental ratio  $K\beta/K\alpha_1 \approx 1.05$  can certainly be reproduced with an intermediate composition of the converter, and most likely with other compositions too, but hitting the experimental number head-on makes little sense when the results cannot be compared to those for the actual converter.

The computation that produces the spectrum in Fig. 1 also puts out spatially resolved spectra shown in Fig. 9. These spectra identify photoelectric absorption as the dominant source of fluorescence. The top two lines give the photon number spectrum  $N(h\nu)$  in 40  $\mu\text{m}$  thin slices of the con-

verter that bracket the region where most of the fluorescence comes from, between the electron entrance at 0.0 mm and at 0.2 mm farther in, at 1/4 of the CSDA range. In these two slices the number spectra are very close and hard to distinguish in black and white. Energetic continuum radiation with energy  $h\nu > 0.3$  MeV is reasonably well approximated by  $N \propto (h\nu)^{-2}$ , the slanted dashed line. The strong effect of photoelectric absorption is visible by the lack of photons from about 0.15 MeV to the K-edge, the vertical dashed line at 69.525 keV.

Where the energy deposition is largest, in the first 0.2 mm, the primary electrons generate so many photons with energies around the K-edge that photoelectric absorption can barely compete: photons with energy just above the K-edge are only 1/3 as numerous as those with energies below the K-edge. However, the incoming electrons stay mostly in the converter's front, and beyond a certain depth they do not refresh the photon number spectrum with new bremsstrahlung. Hence the increased difference between the photon number across the K-edge, to 1/10 and higher, beyond the converter's midpoint. Compton scattering harder photons down to the K-edge is clearly less effective than generating new lower-energy bremsstrahlung photons.

It would be nice if the bremsstrahlung number spectrum  $N(z, h\nu)$  were to factor into two parts,  $N(z, h\nu) = \phi(z)n(h\nu)$ , with a photon number fluence  $\phi(z) = \int d(h\nu)N(z, h\nu)$  and a spectral shape  $n(h\nu) = N/\phi$ , that is, the same for all  $z$ . Such a separation seems to be approximately valid in the converter's front, where most of the fluorescence comes from and  $\phi(z)$  is reasonably constant. However, where such a separation might be more interesting, deep into very thick converters, Fig. 9 shows that the number spectrum does not factor, at least not for range-thick tungsten with monoenergetic 2 MeV electrons.

This and similar computations that are not shown can give superficially surprising results. One example is the dominance of photoionization over ionization by direct electron impact. A thousand electrons produce only about 40  $K\alpha_1$  photons right where they enter, about half as much as the 90  $K\alpha_1$  photons generated by photoionization. However, half-way into the converter the ionization by electron impact is almost exclusively done by Compton electrons and responsible for only 15% of the fluorescence: 85% is from photoionization. This trend continues further toward the converter's back. Another example is the increased bulk attenuation due to the many photon that travel under an angle with the normal.

A quantitative comparison of the measurements with the computations is not attempted, in large part because the primary purpose in this experiment is to make a Cauchois transmission crystal spectrometer perform well in hard bremsstrahlung. The computations should be quite reliable: the bremsstrahlung spectrum's statistics typically had a standard deviation  $\sigma$  much better than 5%, and parameters such as electron source size or inclusion of the detailed fluorescence (with the P-CODES version of ITS) all predict essentially the same results. Moreover, two principal components of the instrumentation, the throughput of the crystal and the calibration of the image plate, had not yet been quantified when this

measurement was done. A future paper<sup>11</sup> contains some of these calibrations, done in support of similar measurements on a warm, dense plasma with a subsequent version of the Cauchois transmission spectrometer, whose redesign was informed by the work reported here.

#### IV. CONCLUSION

The bremsstrahlung continuum generated by multimegavolt electrons in a high atomic number, here tungsten, is largely responsible for the generation of K-shell fluorescence. A properly configured and shielded Cauchois transmission crystal spectrograph can observe tungsten's primary K-shell fluorescence lines despite the accompanying 2 MV end point bremsstrahlung, which is more than two orders of magnitude stronger.

In reflection, when bremsstrahlung from an external source excites the fluorescence, tungsten's  $K\alpha_1$  radiation at 59.3 keV is about twice as strong as the  $K\beta$  radiation at 67.3 keV. However, in forward-directed radiation from a tungsten converter excited by 2 MeV electrons, the intensity of these two fluorescence lines is about the same. To date this anomaly in the fluorescence line ratio  $K\beta/K\alpha_1$ , unity instead of about 0.5, has not been observed or noticed in computations.

The line ratio anomaly is caused by a localized fluorescence source, which is far enough away from the radiation's exit point for differential absorption to become important. Scattering of the electrons by the nuclei in high atomic number materials keeps the electrons close to their entrance point, hence bremsstrahlung production and the generation of fluorescence photons by photoionization are largest where the electrons come in, and negligible on the other side where the fluorescence photons come out. Higher-energy  $K\beta$  radiation from the front of the converter shines through more readily than the lower-energy  $K\alpha_1$  radiation, but still sufficiently well to dominate over fluorescence generated deeper into the converter.

Anomalous line ratios have been seen before,<sup>3</sup> in lower-energy fluorescence photons generated by short-pulse laser irradiation of alloy targets containing silver ( $Z=47$ ) and palladium ( $Z=46$ ). Palladium's K-edge at 24.3 keV is just below the  $K\beta$  line from silver, at about 25 keV. Silver's  $K\beta$  radiation then attenuates strongly on palladium's K-shell electrons, while silver's  $K\alpha$  line at 22 keV and all palladium's fluorescence attenuate through photoelectric absorption in the L-shell of both elements. In the much simpler case of 2 MeV electrons impinging on a cold bremsstrahlung converter, it is possible to compute the radiation generation and transport processes with some accuracy, and the results in this paper support what was surmised already for the laser-alloy interaction experiment: the fluorescence source's location inside the material affects the fluorescence line ratios.

The energy spectrum of the fast electrons from the short-pulse laser<sup>3,20</sup> is insufficiently known to compute the fluorescence source profile. However, these fast electrons

must be much less energetic than 2 MeV, since the modest lead shielding inside the spectrometer was sufficient to suppress the bremsstrahlung that should accompany the fluorescence. For higher power lasers such as the National Ignition Facility, this may no longer be the case.

#### ACKNOWLEDGMENTS

This work was supported by the Army Research Laboratory, Ecopulse's Contract No. W911QX07C0002, and by DTRA's Basic Research Sciences Contract Nos. MIPR 08-2468 and MIPR 09-2156 with the Naval Research Laboratory. N.R.P. thanks R. Kensek (SNL) for discussions about ITS.

<sup>1</sup>H. R. Griem, *Principles of Plasma Spectroscopy* (Cambridge University Press, Cambridge, 1997).

<sup>2</sup>P. M. Nilson, W. Theobald, J. F. Myatt, C. Stoeckl, M. Storm, J. D. Zuegel, R. Betti, D. D. Meyerhofer, and T. C. Sangster, *Phys. Rev. E* **79**, 016406 (2009).

<sup>3</sup>C. I. Szabo, P. Indelicato, A. Gumberidze, G. E. Holland, J. F. Seely, L. T. Hudson, A. Henins, P. Audebert, S. Bastiani-Ceccotti, E. Tabakhoff, and E. Brambrink, *Eur. Phys. J. Spec. Top.* **169**, 243 (2009).

<sup>4</sup>G. P. Williams, Section I in the X-Ray Data Booklet (obtainable from [xdb.lbl.gov](http://xdb.lbl.gov)).

<sup>5</sup>L. T. Hudson, R. D. Deslattes, A. Henins, C. T. Chantler, E. G. Kessler, and J. E. Schweppe, *Med. Phys.* **23**, 1659 (1996).

<sup>6</sup>L. T. Hudson, R. Atkin, C. A. Back, A. Henins, G. E. Holland, J. F. Seely, and C. I. Szabo, *Radiat. Phys. Chem.* **75**, 1784 (2006).

<sup>7</sup>E. O. Baronova, M. M. Stepanenko, and N. R. Pereira, *Rev. Sci. Instrum.* **72**, 1416 (2001).

<sup>8</sup>H. F. Beyer, D. Attia, D. Banas, E.-O. Le Bigot, F. Bosch, J.-Cl. Dousse, E. Förster, A. Gumberidze, S. Hagmann, S. Heß, J. Hoszowska, P. Indelicato, P. Jagodzinski, Chr. Kozhuharov, Th. Krings, D. Liesen, X. Ma, B. Manil, I. Mohos, M. Pajek, D. Proti, R. Reuschl, J. Rzadkiewicz, A. Simionovici, U. Spillmann, Z. Stachura, Th. Stöhlker, M. Trassinelli, S. Trotsenko, A. Warczak, O. Wehrhan, and E. Ziegler, *Spectrochimica Acta, Part B* **64**, 736 (2009).

<sup>9</sup>J. W. Schumer, R. J. Allen, R. J. Commisso, G. Cooperstein, D. D. Hinschelwood, D. P. Murphy, S. J. Stephanakis, S. B. Swanekamp, and F. C. Young, Proceedings of the 15th IEEE International Pulsed Power Conference, Monterey, CA, 2005, p. 1201.

<sup>10</sup>B. V. Weber, R. J. Allen, R. J. Commisso, G. Cooperstein, D. D. Hinschelwood, D. Mosher, D. P. Murphy, P. F. Ottinger, D. G. Phipps, J. W. Schumer, S. J. Stephanakis, S. B. Swanekamp, S. C. Pope, J. R. Threadgold, L. A. Biddle, S. G. Clough, A. Jones, M. A. Sinclair, D. Swatton, T. Carden, and B. V. Oliver, *IEEE Trans. Plasma Sci.* **123**, 4567 (2008).

<sup>11</sup>N. R. Pereira, B. V. Weber, J. P. Apruzese, D. Mosher, J. W. Schumer, J. F. Seely, C. Szabo, C. N. Boyer, and S. J. Stephanakis, "K-line spectra of warm, dense plasmas produced with intense pulsed electron beams," *Rev. Sci. Instrum.* (to be published).

<sup>12</sup>T. Feroli, M. S. Litz, G. Merkel, T. Smith, N. R. Pereira and J. J. Carroll, *Rev. Sci. Instrum.* **80**, 034301 (2009).

<sup>13</sup>J. A. Halbleib and T. A. Mehlhorn, *Nucl. Sci. Eng.* **92**, 338 (1986).

<sup>14</sup>J. Trincavelli and G. Castellano, *Spectrochim. Acta, Part B* **63**, 1 (2008).

<sup>15</sup>A. N. Agnihotri, V. S. Subrahmanyam, R. K. Yadav, R. Shanker, and X. Llovet, *J. Phys. D: Appl. Phys.* **41**, 065205 (2008).

<sup>16</sup>S. G. Gorbics and N. R. Pereira, *Rev. Sci. Instrum.* **64**, 1636 (1993).

<sup>17</sup>J. F. Seely, L. T. Hudson, G. E. Holland, and A. Henins, *Appl. Optics* **47**, 2767 (2008).

<sup>18</sup>J. Jolie and M. Bertschy, *Nucl. Instrum. Methods Phys. Res. B* **95**, 431 (1995).

<sup>19</sup>I. Han, M. Sahin, L. Demir, and Y. Sahin, *Appl. Radiat. Isot.* **65**, 669 (2007).

<sup>20</sup>J. F. Seely, C. I. Szabo, P. Audebert, R. E. Brambrink, E. Tabakhoff, and L. T. Hudson, *Phys. Plasmas* **17**, 023102 (2010).